PCCP

Accepted Manuscript




ROYAL SOCIETY OF CHEMISTRY

www.rsc.org/pccp

Physical Chemistry Chemical Physics RSCPublishing

ARTICLE

# Plasmonic Enhancement of the Optical Absorption and Catalytic Efficiency of $BiVO_4$ Photoanodes Decorated with $Ag@SiO_2$ Core-Shell Nanoparticles

Fatwa F. Abdi,[ab] Ali Dabirian,[c] Bernard Dam,[b] and Roel van de Krol[a]

Cite this: DOI: 10.1039/x0xx00000x

Received 00th January 2014,
Accepted 00th January 2014

DOI: 10.1039/x0xx00000x

www.rsc.org/

Recent progress in the development of bismuth vanadate ($BiVO_4$) photoanodes has firmly established it as a promising material for solar water splitting applications. Performance limitations due to intrinsically poor catalytic activity and slow electron transport have been successfully addressed through the application of water oxidation co-catalysts and novel doping strategies. The next bottleneck to tackle is the modest optical absorption in $BiVO_4$, particularly close to its absorption edge of 2.4 eV. Here, we explore the modification of the $BiVO_4$ surface with $Ag@SiO_2$ core-shell plasmonic nanoparticles. A photocurrent enhancement by a factor of ~2.5 is found under 1 sun illumination (AM1.5). We show that this enhancement consists of two contributions: optical absorption and catalysis. The optical absorption enhancement is induced by the excitation of localized surface plasmon resonances in the Ag nanoparticles, and agrees well with our full-field electromagnetic simulations. Far-field effects (scattering) are found to be dominant, with a smaller contribution from near-field plasmonic enhancement. In addition, a significant catalytic enhancement is observed, which is tentatively attributed to the electrocatalytic activity of the $Ag@SiO_2$ nanoparticles.

In the field of solar water splitting, bismuth vanadate ($BiVO_4$) has emerged as one of the most promising photoanode materials. The monoclinic scheelite phase (clinobisvanite) is the most photo-active form of $BiVO_4$.The material shows n-type conductivity and has a bandgap of ~2.4 eV.[1-3] An attractive aspect of $BiVO_4$ is that its band edge positions are more favorably located than other well-known metal oxides for solar water splitting, such as hematite or tungsten trioxide.[4-6] $BiVO_4$ photoanodes profit from a good stability in aqueous solutions with pH values between 3 and 11.[7] However, the performance of the material is hampered by two main limitations: (i) slow hole transfer across the semiconductor/electrolyte interface (i.e., low catalytic activity for water oxidation) and (ii) slow electron transport, which results in sub-optimal carrier separation. In recent years, these issues have successfully been addressed. The first issue has been largely solved by attaching co-catalysts to the surface of $BiVO_4$. Oxygen evolution catalysts such as $RhO_2$,[8] cobalt phosphate (Co-Pi),[9-11] cobalt borate (Co-Bi),[12] nickel borate (Ni-Bi),[13] and iron oxyhydroxide (FeOOH)[14] have been successfully used. At sufficiently high bias potentials, catalytic activities of up to 100% have been shown,[9, 11, 15] demonstrating that the problem of slow water oxidation catalysis has been solved for $BiVO_4$. The second limitation (slow electron transport) can be solved by introducing a donor-type dopant, such as W and Mo,[9, 11, 15-18] thereby increasing the carrier concentration. Recently, we have shown that this can be further improved by introducing a gradient in the dopant concentration in $BiVO_4$. The gradient dopant profile introduces a small but effective electrical potential gradient in the film, which improves the carrier separation efficiency to values as high as 80%.[19] With these modifications an AM1.5 photocurrent of 3.6 mA/cm$^2$ has been achieved at 1.23 V vs the reversible hydrogen electrode (RHE),

which firmly establishes $BiVO_4$ as the currently highest performing metal oxide photoanode.[19]

With the catalysis and charge transport issues solved, modest light absorption—especially for photons with energies close to the bandgap—becomes the next main bottleneck. To illustrate this, if we assume that all the light absorbed in our best-performing W:$BiVO_4$ samples contributes to photocurrent, we would still *only* have ~5 mA/cm$^2$.[19] For comparison, the maximum theoretical photocurrent for $BiVO_4$ is ~7.5 mA/cm$^2$ (assuming that all photons with an energy higher than the bandgap are absorbed and collected). This means that a significant increase of the photocurrent (2.5 mA/cm$^2$) can be achieved by improving light absorption. Unfortunately, simply increasing the thickness of the film to absorb more light will not work, since the carrier diffusion length in $BiVO_4$ is ~100 nm.[20, 21] Considering that the best-performing $BiVO_4$ already has a thickness of ~200 nm, other strategies to improve light absorption are therefore needed.

Recently, surface plasmon resonances of metallic nanostructures, such as Au, Ag, and Al, have been extensively used to improve the absorption—and the efficiency—in various photocatalytic systems and solar cells.[22-26] The same approach has also been pursued for solar water splitting applications.[27-33] For example, Thimsen et al. reported a significant improvement of the optical absorption in hematite when Au plasmonic nanoparticles are introduced on the hematite surface or at the interface between the substrate and hematite film.[28] However, this improvement is not accompanied by the same improvement in the overall efficiency; the photocurrent was found to decrease instead. This inconsistency is attributed to the introduction of traps at the interface between the Au and hematite. One way to circumvent this problem is by introducing a thin $SiO_2$ insulating layer on the surface of the Au nanoparticles. Thomann et al. demonstrated that this effectively prevents nanoparticle-induced charge recombination.[29]

In this paper, we explore the application of core-shell nanoparticles on the surface of 100 nm-thick spray-deposited $BiVO_4$ films as a route to enhance the optical absorption in the films. Similar to the approach of Thomann et al.,[29] $SiO_2$ is used as the insulating layer around the core metal. However, here, Ag is used as the core metal because: (i) Ag is less expensive than Au, and (ii) the plasmon frequency of Ag can be tailored between 400 to 600 nm,[34, 35] providing a better match to the absorption spectrum of $BiVO_4$. We predict and show the beneficial effect of the Ag@$SiO_2$ core-shell nanoparticles on the performance of $BiVO_4$ photoanodes. Through a detailed photoelectrochemical analysis, we are able to distinguish between absorption and catalytic effects that contribute to the observed improvements. To the best of our knowledge, this is the first report on the application of core-shell nanoparticles to improve the absorption and efficiency of $BiVO_4$ photoanodes.

We first perform full-field electromagnetic simulations to assess the performance enhancements of Ag@$SiO_2$ nanoparticles on $BiVO_4$ films. In these simulations, we numerically solve frequency-domain Maxwell equations using a finite element method, following a previously reported approach.[29, 36] We consider two different types of $BiVO_4$ samples: (i) bare $BiVO_4$ and (ii) $BiVO_4$ decorated with Ag@$SiO_2$ core-shell nanoparticles (Ag@$SiO_2$/$BiVO_4$), both are shown in Figure 1. The diameter of the Ag core is 50 nm, and the thickness of the $SiO_2$ shell is 10 nm, based on TEM analysis of the nanoparticles (see ESI, Figure S1†). To make our calculations as realistic as possible, we explicitly take into account the surface roughness of the films in relation to the Ag@$SiO_2$ particle size. The surface roughness was measured with atomic force microscopy (see ESI, Figure S2†).

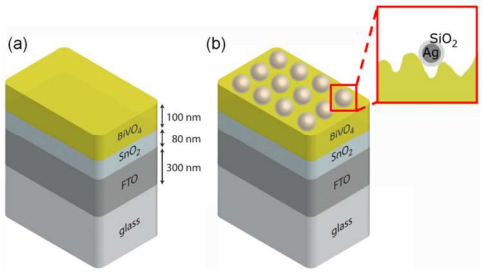


**Figure 1.** Schematic illustration of the **(a)** bare and **(b)** Ag@$SiO_2$ decorated $BiVO_4$ (Ag@$SiO_2$/$BiVO_4$) samples.

The direct results of the electromagnetic calculations are the amplitudes of the electric and magnetic fields ($E$, $H$). Based on these, we calculate the rate of light absorption at every point inside the light absorbing layer, using the following equation:

$$P_d = \frac{1}{2}\omega\varepsilon''(\omega)\left|\overline{E}(\overline{r},\omega)\right|^2 \quad (1)$$

Here, $\omega$ is the angular frequency of the incident light, $\varepsilon''(\omega)$ is the imaginary part of the permittivity of the material, and $\left|\overline{E}(\overline{r},\omega)\right|$ describes the amplitude of the electric field at position $r$ and angular frequency $\omega$. Inside the $BiVO_4$, the power-loss density ($P_d$) is the rate of electron-hole pair generation at every point (in W/m$^3$), while in the Ag nanoparticles, it describes the absorbed photons that dissipate their energy as phonons.

Figure 2 shows the distribution of $P_d$ at the cross-section of the different samples under illumination with 465 nm light, given an incident power of 1 W. The photoanode is illuminated from the substrate side (back-side illumination). Non-zero optical absorption takes place only within Ag and $BiVO_4$ since other layers in the structure do not absorb 465 nm light. Note that the absorption profile over the bare $BiVO_4$ (Figure 2a) is not uniform, despite the planar wave-front of the excitation light. This is caused by the wavelength-scale dimensions of the superficial features of $BiVO_4$, which affect the propagation of light.[37] Such wavelength-scale features can have Mie resonances and, if properly engineered, can be used to reduce the reflectance from the layer.[37] Figure 2b and c shows a $BiVO_4$ film segment with a single Ag@$SiO_2$ nanoparticle, which corresponds to a 25% surface coverage. Results from the two conditions were averaged to take the random position of Ag@$SiO_2$ into consideration. The absorption in the $BiVO_4$ is enhanced, especially in the area underneath the nanoparticle.



 

Further increase of the surface coverage to up to 50% (Figure 2d) results in an even stronger absorption enhancement.

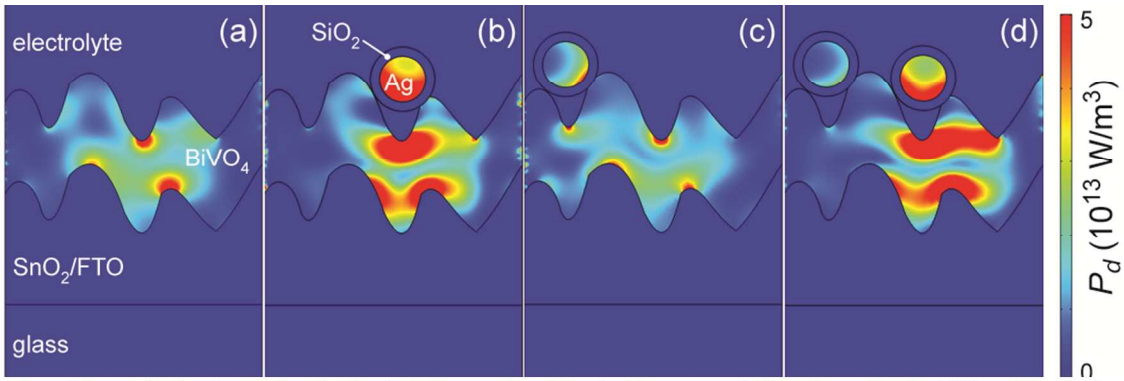


**Figure 2.** Color plots of the amplitude of power-loss density, $P_d$, in the samples with an incident power of 1 W and wavelength of 465 nm. The illumination direction is from the bottom (back-side of the samples). Bare $BiVO_4$ is shown in **(a)**. $BiVO_4$ with 25% surface coverage of $Ag@SiO_2$ are shown in **(b)** and **(c)**, which are averaged to take the position of the nanoparticle into consideration. Finally, $BiVO_4$ with 50% surface coverage of $Ag@SiO_2$ nanoparticles is shown in **(d)**.

The total absorptance in the $BiVO_4$ film is calculated by integrating $P_d$ over the entire volume of $BiVO_4$, according to the following equation:

$$A(\lambda) = \frac{\int_{BiVO_4\ volume} P_d(\bar{r},\lambda) d^3\bar{r}}{P_{inc}} \quad (2)$$

where $P_{inc}$ is the power of the incident light. Figure 3a shows the calculated absorption spectra of $BiVO_4$ films with 0%, 25% and 50% surface coverage of $Ag@SiO_2$ nanoparticles. A near-field enhancement effect can be identified by the presence of peaks in the absorption spectrum, corresponding to the plasmonic resonance(s) of the nanoparticles.[22, 29] Our simulation based on a small area in $BiVO_4$ adjacent to the nanoparticle shows that we would expect a sharp peak between 410 and 420 nm (see ESI, Figure S3†). However, we observe a broadband enhancement in Figure 3a, i.e., it is not specific to a certain wavelength range. We therefore conclude that effects other than near-field enhancement must also play a role. One possible explanation is the occurrence of light scattering from the $Ag@SiO_2$ nanoparticles and/or from the surface features of the $BiVO_4$ layer. Optical scattering, which can be classified as a far-field effect, is indeed known to enhance the absorption under the right conditions.[38] Indeed, the scattering cross-section of the $Ag@SiO_2$ nanoparticle used here is much higher than its absorption cross-section (see ESI, Figure S4†).

Figure 3b shows the calculated absorption enhancement—integrated over the AM1.5 spectrum—as a function of the surface coverage. A maximum is found between 40-60%. At higher coverage, the optical dissipation in Ag becomes larger than the plasmonic induced optical absorption in $BiVO_4$; hence, smaller absorption enhancement is observed. Based on this, we covered~50% of the surface of our 100 nm-thick, spray pyrolysed $BiVO_4$ film with the $Ag@SiO_2$ nanoparticles. To obtain this coverage we used ~2.5 μL/cm$^2$ of the solution of $Ag@SiO_2$ nanoparticles. The optical density and the particle size distribution of the solution are shown in the ESI, Figure S5†. Detailed sample preparation and characterization procedures can be found in the ESI†. Our SEM analysis shows that the coverage is not perfectly uniform (see ESI, Figure S6†). Nevertheless, the overall coverage is estimated to be 35-45%, which is close to the desired coverage.

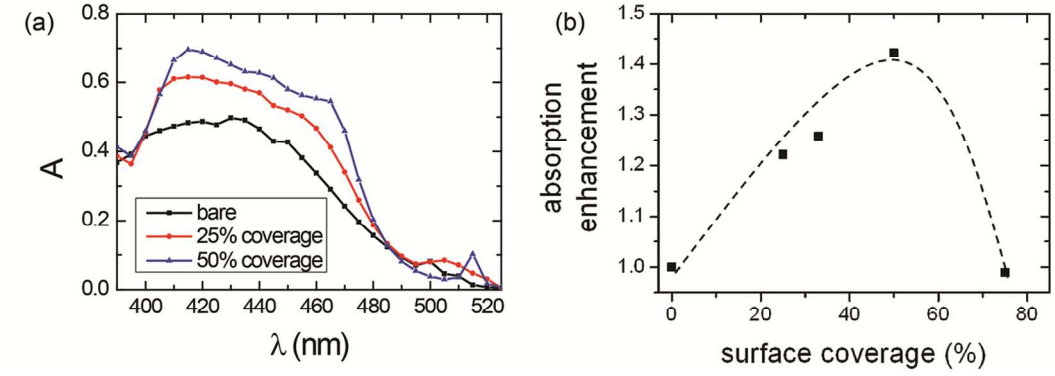


**Figure 3. (a)** Simulated absorption of $BiVO_4$ with 0% (bare), 25% and 50% surface coverage of $Ag@SiO_2$ nanoparticles. **(b)** The calculated absorption enhancement as a function of the $BiVO_4$ surface coverage with $Ag@SiO_2$ nanoparticles.

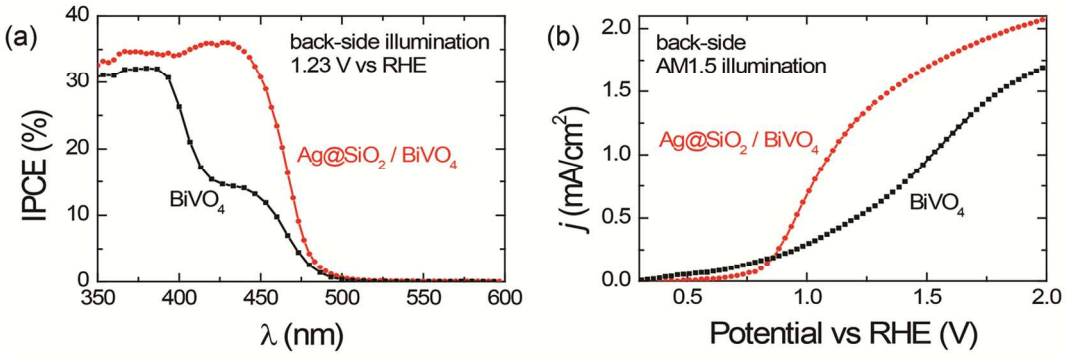


**Figure 4. (a)** Incident photon-to-current efficiencies (IPCE) and **(b)** AM1.5 photocurrents of bare and $Ag@SiO_2/BiVO_4$. The illumination direction is from the substrate side of the samples. The IPCE values were measured at 1.23 V vs RHE.

Figure 4a shows the IPCE of the bare $BiVO_4$ and the $Ag@SiO_2/BiVO_4$ at 1.23 V vs RHE under back-side illumination. Upon decoration with $Ag@SiO_2$, the IPCE of the $BiVO_4$ photoanode is greatly improved at wavelengths larger than 400 nm. This agrees well with our simulations, and is consistent with optical absorption measurements on these same samples (see ESI, Figure S7†). The same broadband enhancement between 400 and 500 nm is also observed, which confirms that both near- and far-field effects play important roles in the enhancement mechanism.

The increase in IPCE is also reflected in the AM1.5 photocurrent, shown in Figure 4b. A photocurrent of ~1.4 $mA/cm^2$ at 1.23 V vs RHE is achieved for $Ag@SiO_2/BiVO_4$. This is a ~2.5-fold improvement compared to bare $BiVO_4$. To the best of our knowledge, this is one of the highest AM1.5 photocurrent enhancements reported for a photoanode decorated with metal plasmonic nanoparticles.[28-33]

To ensure that the observed photocurrent is not a result of photocorrosion or oxidation of the sample, we investigated the stability of $Ag@SiO_2/BiVO_4$ under illumination. Figure 5 shows the chronoamperometry measurement of the $Ag@SiO_2/BiVO_4$ sample, at 1.23 V vs RHE under back-side chopped AM1.5 illumination. The stability of the sample is excellent, with no noticeable degradation in 25 minutes. Integration of the photocurrent gives a total charge of 1125 $mC/cm^2$, which is ~10 times larger than the charge that would be needed to photo-corrode the nanoparticles. This proves that the photocurrent enhancement can indeed be attributed to improved performance of the $Ag@SiO_2$-modified photoelectrode.

The 2.5-fold photocurrent improvement we observed is, however, much higher than the ~40% enhancement (Fig. 3b) that is predicted by integrating the calculated absorptance over the AM1.5 irradiance.[36] To reconcile this, a thorough photo-electrochemical analysis of the modified $BiVO_4$ films was performed. The total enhancement factor ($f$) that is induced by the $Ag@SiO_2$ nanoparticles can be written as:

$$f = \frac{J_{Ag@SiO_2/BiVO_4}}{J_{BiVO_4}} \quad (3)$$

$J_{Ag@SiO_2/BiVO_4}$ and $J_{BiVO_4}$ are the photocurrents of $Ag@SiO_2/BiVO_4$ and bare $BiVO_4$, respectively. We now assume that the enhancement can be caused by the increased absorption in $BiVO_4$ (as a result of plasmonic resonances and scattering) as well as surface catalytic effects. To isolate the absorption enhancement, $H_2O_2$ was added to the electrolyte to serve as a very effective hole scavenger. Recent studies have shown that the efficiency of hole injection into the electrolyte is ~100% in the presence of $H_2O_2$.[11, 39] Under these conditions, it is reasonable to assume that catalysis and surface recombination no longer play a significant role, and that the photocurrent enhancement is entirely due to absorption effects:

$$f_{abs} = \frac{J_{Ag@SiO_2/BiVO_4+H_2O_2}}{J_{BiVO_4+H_2O_2}} \quad (4)$$

where $J_{Ag@SiO_2/BiVO_4+H_2O_2}$ and $J_{BiVO_4+H_2O_2}$ are the photocurrents of $Ag@SiO_2/BiVO_4$ and bare $BiVO_4$ in the presence of $H_2O_2$, respectively. The catalytic enhancement is obtained by dividing the total enhancement by the absorption enhancement:

$$f_{cat} = \frac{f}{f_{abs}} \quad (5)$$

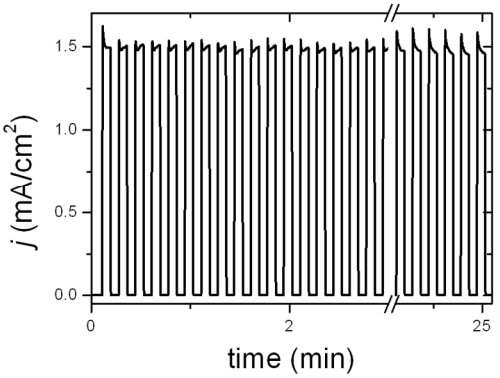


**Figure 5.** Chronoamperometry plot of $Ag@SiO_2/BiVO_4$ under back-side chopped AM1.5 illumination at 1.23 V vs RHE.

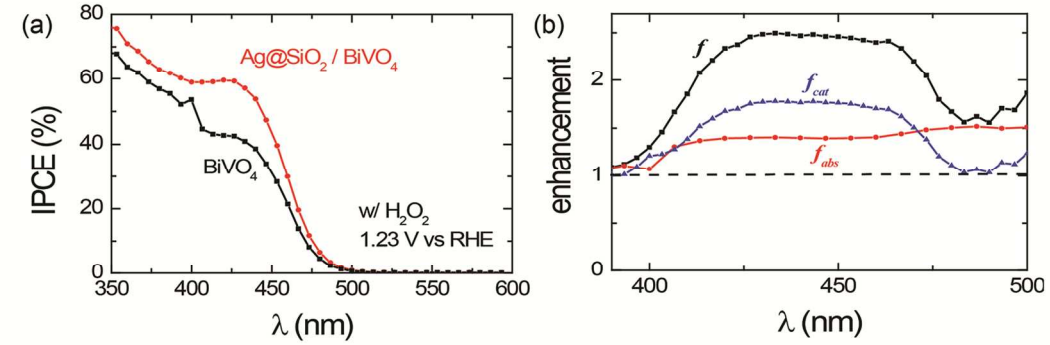


**Figure 6. (a)** IPCE of bare $BiVO_4$ and $Ag@SiO_2/BiVO_4$ at 1.23 V vs RHE in the presence of 0.5 M $H_2O_2$ in the electrolyte. **(b)** Absorption ($f_{abs}$), catalytic ($f_{cat}$) and total enhancements ($f$) in $Ag@SiO_2/BiVO_4$ as a function of excitation wavelength.

Figure 6a shows the IPCE of the bare and $Ag@SiO_2/BiVO_4$ in the presence of $H_2O_2$ at 1.23 V vs RHE. The enhancement occurs in the same spectral region as in Figure 4a, but it is significantly smaller. From the data in Figs. 4a and 6a, the absorption, catalytic and total enhancements are calculated from Eqs. 3-5 and shown in Figure 6b. Integration of the absorption enhancement over the AM1.5 spectrum gives an overall enhancement of ~33%, which closely matches the predicted enhancement from our full-field electromagnetic simulations. A similar enhancement (~28% at 1.23 V vs RHE) is observed when we compare the photocurrents of bare $BiVO_4$ and $Ag@SiO_2/BiVO_4$ in the presence of $H_2O_2$ under actual AM1.5 illumination (see ESI, Figure S8†).

Figure 6b clearly shows that the catalytic enhancement is significantly larger than the absorption enhancement. In order to shed light on the cause of this catalytic enhancement, we determined the catalytic and carrier separation efficiencies of the bare $BiVO_4$ and $Ag@SiO_2/BiVO_4$ (see ESI, Figure S9†).[11] The carrier separation efficiencies of both samples are found to be identical, which proves that the enhancement cannot be attributed to the formation of a rectifying junction between the $Ag@SiO_2$ and the $BiVO_4$. In contrast, the catalytic efficiency for the $Ag@SiO_2/BiVO_4$ sample is ~85% larger than for the bare $BiVO_4$ sample at 1.23 V vs. RHE. We tentatively attribute this difference to the electrocatalytic activity of $Ag@SiO_2$ nanoparticles on the surface of $BiVO_4$. At low potentials (< 0.9 vs RHE), the catalytic efficiency of $Ag@SiO_2/BiVO_4$ is lower than that of the bare sample. In this case, $Ag@SiO_2$ nanoparticles are inactive as catalyst; they just block part of the $BiVO_4$ surface, which explains the lower catalytic efficiency (Fig. S9). This is also evident in Fig. 4b, where the photocurrent of the $Ag@SiO_2/BiVO_4$ is lower than that of the bare $BiVO_4$. The situation is, however, reversed at higher potentials where the catalytic efficiency of $Ag@SiO_2/BiVO_4$ exceeds that of bare $BiVO_4$. It appears that at these potentials the $Ag@SiO_2$ nanoparticles no longer block charge transfer and, instead, catalyze the water oxidation reaction. While there have been no reports of their catalytic activity for water oxidation, redox catalysis using $Ag@SiO_2$ and $Ag\text{-}SiO_2$ composites have been reported.[40, 41] To confirm this, we deposited the $Ag@SiO_2$ core-shell nanoparticles on the surface of an FTO substrate. We then compare the dark current of this $Ag@SiO_2$/FTO and a bare FTO substrate as a function of potential (see ESI, Figure S10†), and observe a ~200 mV cathodic shift of the onset potential for the $Ag@SiO_2$/FTO. This shows that $Ag@SiO_2$ indeed behaves as a (dark) catalyst for water oxidation.

One surprising and counter-intuitive observation from Fig. 6b is that the catalytic enhancement shows a pronounced dependence on wavelength. Although the exact reason for this is unclear at the moment, we note that the center of the spectral region where catalytic enhancement occurs overlaps exactly with the optical absorbance of the $Ag@SiO_2$ nanoparticles (Fig. S5a). We therefore speculate that the electric field that propagates from the $Ag@SiO_2$ nanoparticles aids the water oxidation reaction, for example by enhancing the carrier separation efficiency near the surface,[42] or through plasmon-induced resonant energy transfer (PIRET).[43] Further investigation is needed to elucidate this, which is beyond the scope of the current work.

## Conclusions

In summary, we have explored the application of $Ag@SiO_2$ core-shell nanoparticles on the surface of $BiVO_4$ to improve the absorption in $BiVO_4$. By performing a thorough photoelectrochemical analysis with an efficient hole scavenger, we can distinguish absorption and catalytic contributions to the observed enhancement. The absorption enhancement (~33%) is mostly due to far-field effects (scattering), with a smaller contribution due to near-field localized surface plasmon resonances. This is markedly different from the mechanism in smaller (<20 nm) metal plasmonic nanoparticles, where near-field effects dominate.[43] The experimental results agree well with the full-field electromagnetic simulations. The catalytic enhancement is twice as large as the absorption enhancement, and is tentatively assigned to the improvement of water oxidation kinetics due to the catalytic activity of $Ag@SiO_2$

nanoparticles. The effects combine to give a ~2.5-fold improvement of AM1.5 photocurrent at 1.23 V vs RHE, which is one of the highest photocurrent enhancements reported for a photoanode decorated with capped metal plasmonic nanoparticles. Such a large improvement is crucial for the development of $BiVO_4$ photoanodes, since modest absorption—especially for wavelengths close to the band edge—has been identified as one of the main performance-limiting factors.

## Acknowledgements

We gratefully acknowledge the European Commission's Framework Project 7 (NanoPEC, Project 227179) for financial support of this work. We thank Ulrike Bloeck for the TEM imaging. F.F.A. thanks Dr. Andrea Baldi for valuable discussions.

## Notes and references

[a] Helmholtz-Zentrum Berlin für Materialien und Energie Gmbh, Institute for Solar Fuels, Hahn-Meitner-Platz 1, 14109 Berlin, Germany.
E-mail:fatwa.abdi@helmholtz-berlin.de

[b] Materials for Energy Conversion and Storage (MECS), Department of Chemical Engineering, Delft University of Technology, P.O. Box 5045, 2600 GA Delft, The Netherlands.

[c] Department of Physics, Sharif University of Technology, 14588, Tehran, Iran. Present address: Photovoltaics and Thin Film Electronics Laboratory, Ecole Polytechnique Federale de Lausanne (EPFL), Rue de Maladière 71 (Microcity), 2000 Neuchâtel, Switzerland

† Electronic Supplementary Information (ESI) available: experimental procedures, Figures S1-10. See DOI: 10.1039/b000000x/

1. A. Kudo, K. Omori and H. Kato, *J. Am. Chem. Soc.*, 1999, **121**, 11459-11467.
2. A. Kudo, K. Ueda, H. Kato and I. Mikami, *Catal. Lett.*, 1998, **53**, 229-230.
3. S. Tokunaga, H. Kato and A. Kudo, *Chem. Mater.*, 2001, **13**, 4624-4628.
4. R. van de Krol, Y. Q. Liang and J. Schoonman, *J. Mater. Chem.*, 2008, **18**, 2311-2320.
5. S. J. Hong, S. Lee, J. S. Jang and J. S. Lee, *Energy Environ. Sci.*, 2011, **4**, 1781-1787.
6. S. Chen and L. W. Wang, *Chem. Mater.*, 2012, **24**, 3659-3666.
7. F. F. Abdi, N. Firet, A. Dabirian and R. van de Krol, *MRS Online Proceedings Library*, 2012, **1446**, mrss12-1446-u1402-1405.
8. W. J. Luo, Z. S. Yang, Z. S. Li, J. Y. Zhang, J. G. Liu, Z. Y. Zhao, Z. Q. Wang, S. C. Yan, T. Yu and Z. G. Zou, *Energy Environ. Sci.*, 2011, **4**, 4046-4051.
9. D. K. Zhong, S. Choi and D. R. Gamelin, *J. Am. Chem. Soc.*, 2011, **133**, 18370-18377.
10. F. F. Abdi and R. van de Krol, *J. Phys. Chem. C*, 2012, **116**, 9398-9404.
11. F. F. Abdi, N. Firet and R. van de Krol, *ChemCatChem*, 2013, **5**, 490-496.
12. C. Ding, J. Shi, D. Wang, Z. Wang, N. Wang, G. Liu, F. Xiong and C. Li, *Phys. Chem. Chem. Phys.*, 2013, **15**, 4589-4595.
13. S. K. Choi, W. Choi and H. Park, *Phys. Chem. Chem. Phys.*, 2013.
14. J. A. Seabold and K. S. Choi, *J. Am. Chem. Soc.*, 2012, **134**, 2186-2192.
15. H. W. Jeong, T. H. Jeon, J. S. Jang, W. Choi and H. Park, *J. Phys. Chem. C*, 2013, **117**, 9104-9112.
16. S. P. Berglund, A. J. E. Rettie, S. Hoang and C. B. Mullins, *Phys. Chem. Chem. Phys.*, 2012, **14**, 7065-7075.
17. K. P. S. Parmar, H. J. Kang, A. Bist, P. Dua, J. S. Jang and J. S. Lee, *ChemSusChem*, 2012, **5**, 1926-1934.
18. S. K. Pilli, T. E. Furtak, L. D. Brown, T. G. Deutsch, J. A. Turner and A. M. Herring, *Energy Environ. Sci.*, 2011, **4**, 5028-5034.
19. F. F. Abdi, L. Han, A. H. M. Smets, M. Zeman, B. Dam and R. van de Krol, *Nat. Commun.*, 2013, **4:2195**, 1-7.
20. F. F. Abdi, T. J. Savenije, M. M. May, B. Dam and R. van de Krol, *J. Phys. Chem. Lett.*, 2013, **4**, 2752-2757.
21. A. J. E. Rettie, H. C. Lee, L. G. Marshall, J. F. Lin, C. Capan, J. Lindemuth, J. S. McCloy, J. Zhou, A. J. Bard and C. B. Mullins, *J. Am. Chem. Soc.*, 2013, **135**, 11389-11396.
22. H. A. Atwater and A. Polman, *Nat. Mater.*, 2010, **9**, 205-213.
23. V. E. Ferry, L. A. Sweatlock, D. Pacifici and H. A. Atwater, *Nano Lett.*, 2008, **8**, 4391-4397.
24. S. Pillai, K. Catchpole, T. Trupke and M. Green, *J. Appl. Phys.*, 2007, **101**, 093105.
25. S. Linic, P. Christopher and D. B. Ingram, *Nat. Mater.*, 2011, **10**, 911-921.
26. W. Hou and S. B. Cronin, *Adv. Funct. Mater.*, 2013, **23**, 1612-1619.
27. S. C. Warren and E. Thimsen, *Energy Environ. Sci.*, 2012, **5**, 5133-5146.
28. E. Thimsen, F. Le Formal, M. Grätzel and S. C. Warren, *Nano Lett.*, 2010, **11**, 35-43.
29. I. Thomann, B. A. Pinaud, Z. Chen, B. M. Clemens, T. F. Jaramillo and M. L. Brongersma, *Nano Lett.*, 2011, **11**, 3440-3446.
30. R. Solarska, A. Krolikowska and J. Augustynski, *Angew. Chem., Int. Ed.*, 2010, **49**, 7980-7983.
31. J. Lee, S. Mubeen, X. Ji, G. D. Stucky and M. Moskovits, *Nano Lett.*, 2012, **12**, 5014-5019.
32. A. Valdes, J. Brillet, M. Gratzel, H. Gudmundsdottir, H. A. Hansen, H. Jonsson, P. Klupfel, G.-J. Kroes, F. Le Formal, I. C. Man, R. S. Martins, J. K. Norskov, J. Rossmeisl, K. Sivula, A. Vojvodic and M. Zach, *Phys. Chem. Chem. Phys.*, 2012, **14**, 49-70.
33. H. Gao, C. Liu, H. E. Jeong and P. Yang, *ACS Nano*, 2012, **6**, 234-240.
34. T. R. Jensen, M. D. Malinsky, C. L. Haynes and R. P. Van Duyne, *J. Phys. Chem. B*, 2000, **104**, 10549-10556.
35. Y. Sun and Y. Xia, *Analyst*, 2003, **128**, 686-691.
36. M. Akbari, M.-R. Kikhavani, K. Sheshyekani and A. Dabirian, *RSC Adv.*, 2013, **3**, 17837-17842.
37. P. Spinelli, M. A. Verschuuren and A. Polman, *Nat. Commun.*, 2012, **3**, 692.
38. K. Catchpole and A. Polman, *Appl. Phys. Lett.*, 2008, **93**, 191113.
39. H. Dotan, K. Sivula, M. Gratzel, A. Rothschild and S. C. Warren, *Energy Environ. Sci.*, 2011, **4**, 958-964.
40. T. Ung, L. M. Liz-Marzán and P. Mulvaney, *J. Phys. Chem. B*, 1999, **103**, 6770-6773.
41. L. Jin, K. Qian, Z. Jiang and W. Huang, *J. Mol. Catal. A: Chem.*, 2007, **274**, 95-100.
42. L. Li, P. A. Salvador and G. S. Rohrer, *Nanoscale*, 2014, **6**, 24-42.
43. S. K. Cushing and N. Wu, *Electrochem. Soc. Interface*, 2013, 63.



 